Science of the Total Environment 408 (2010) 3477–3489

Contents lists available at ScienceDirect

Science of the Total Environment

journal homepage: www.elsevier.com/locate/scitotenv

Effect of dissolved organic matter on the stability of magnetite nanoparticles under different pH and ionic strength conditions

Jun-Dong Hu [a,1], Yuniati Zevi [b,2], Xiao-Ming Kou [c], John Xiao [c], Xue-Jun Wang [a,*], Yan Jin [b,*]

[a] Laboratory for Earth Surface Processes (LASP), College of Urban and Environmental Sciences, Peking University, Beijing, 100871, China
[b] Environmental Soil Physics Lab, Department of Plant and Soil Sciences, University of Delaware, Newark, Delaware, 19716, USA
[c] Electromagnetic Materials Laboratory, Department of Physics and Astronomy, University of Delaware, Newark, Delaware, 19716, USA

ARTICLE INFO

Article history:
Received 27 July 2009
Received in revised form 23 February 2010
Accepted 19 March 2010
Available online 24 April 2010

Keywords:
Engineered nanoparticle
Magnetite
Aggregation
Stability kinetics
Humic acid
DLVO theory
AFM

ABSTRACT

Upon release of engineered nanoparticles (NPs) into the subsurface environment, their fate and transport and hence their potential environmental and public health impacts will largely depend on how stable these NPs are as suspended particles in the natural environment. In this study, we systematically examine the effect of humic acid (HA) on surface charge status and aggregation potential of magnetite (Fe_3O_4) NPs, selected as a model for metal oxide NPs, over a wide range of solution pH and ionic strength. Through zeta potential (ZP) measurements, we found that HA can adsorb to magnetite particles hence modifying their surface charge status. At low loadings, the presence of HA can induce a shift in the point zero of charge of due to partial neutralization of the positive charges on magnetite NPs. At high loadings, however, HA is capable of completely cover magnetite particles giving rise to a suspension ZP profile similar to its own (observed in presence of 20 mg L^{-1} HA). These impacts on surface charge correspond well with the observed aggregation behaviors in the absence and presence of HA. From the dynamic light scattering (DLS) measurements, fast aggregation, which is independent of solution chemistry, took place when the pH is close to the point zero charge (PZC) and the ionic strength is above the critical coagulation concentration (*CCC*). At high ionic strength, a small dose (2 mg L^{-1}) of HA stabilized the NPs' suspension significantly. This stabilization effect is substantially enhanced with increasing HA concentration. The calculated DLVO (Derjaguin–Landau–Verwey–Overbeek) interaction energy profiles, using experimentally determined values of Hamaker constant, adequately support the experimental observations. The DLVO analysis further reveals the possible presence of secondary energy minima and the possibility of deaggregation of magnetite agglomerates. The complexation of HA–NPs and the HA effects on NPs aggregations were confirmed by atomic force microscope (AFM) observations.

1. Introduction

With increasing development and wide range applications of engineered nanoparticles (NPs), release of these NPS into the environment is unavoidable (Guardia et al., 2007; Hristovski et al., 2007; Hu et al., 2004; Kim and Walker, 2001; Oberdorster et al., 2005; Si et al., 2005; Wei and Viadero, 2007). Upon releases, mobile NPs have the potential to act as carriers of contaminants (e.g., strongly sorbing organic compounds, heavy metals, pesticides, etc.) or pose environmental and public health concern themselves. In natural porous systems (e.g. soils and groundwater aquifers), stability of NPs, i.e., whether they will remain in suspension as small particles, will control the transport and fate of these particles and other adsorbed contaminants. Therefore, understanding how engineered NPs exist and transport in the subsurface porous media is of fundamental importance to providing accurate assessment of potential environmental, ecological, and public health impacts of engineered NPs upon their release into the environment.

The study of stability and aggregation kinetics of colloid has been an important aspect of colloid science for many decades. Studies have found that solution pH, ionic strength and natural organic matter (NOM) loading are the main factors affecting surface charge status of colloids hence their stability and transport behavior in the subsurface environments (Christian et al., 2008; Jekel, 1986; Ojamae et al., 2006; Tipping and Higgins, 1982; Tombacz et al., 1999). Although similar studies using engineered NPs have began to emerge their behavior under relevant environmental conditions in subsurface media remains largely unknown. In particular, mechanistic investigation of aggregation kinetics of NPs under the influence of NOM is especially lacking.

A number of studies have been conducted to evaluate the aggregation behavior, hence the stability of micro- and nano-scale

* Corresponding authors. Wang is to be contacted at Tel./fax: +86 10 62754091. Jin, Tel.: +1 302 831 6962; fax: +1 302 831 0605.
E-mail addresses: xjwang@urban.pku.edu.cn (X.-J. Wang), yjin@udel.edu (Y. Jin).
[1] Tel./fax: +86 10 62754091.
[2] Tel.: +1 302 831 6962; fax: +1 302 831 0605.

0048-9697/$ – see front matter © 2010 Elsevier B.V. All rights reserved.
doi:10.1016/j.scitotenv.2010.03.033

particles via dynamic light scattering (DLS), by which the average hydrodynamic size of suspended particles can be determined as a function of time. Particle aggregate size has been found to increase with increasing concentration of background electrolyte, and that particle suspension destabilization (i.e., aggregation) occurs at pH values in the vicinity of NPs point of zero charge (pH_{pzc}) (He et al., 2008; Illés and Tombácz, 2006). Aggregation kinetics can be experimentally determined and is generally characterized with two stages or regimes: fast and slow aggregations. The fast aggregation regime, which is diffusion-limited, occurs in the early stage of an aggregation process and its aggregation rate constant does not depend on parameters such as solution pH and ionic strength. On the other hand, the slow aggregation regime, which is reaction-limited, takes place before the fast aggregation stage and the aggregation rate constant is lower and strongly depends on pH and ionic strength. The transition point between these two regimes is defined as the critical coagulation concentration (*CCC*). Berka and Rice (2004) reported that in the slow aggregation regime (Borkovec and Behrens, 2006), with increasing concentration of NaCl, kaolinite (<0.2 μm size) particle suspension became more unstable. When NaCl concentration reached the *CCC*, rapid aggregation took place, and the aggregation process was independent of ionic strength above the *CCC*.

Humic substances are the major organic constituents of soil and aquatic environments and therefore play an important role in influencing fate and transport of colloidal particles. Many investigations have revealed that relatively small amount of organic anions absorbed on Al–OH/Fe–OH surface sites of minerals can induce a significant increase in the stability of dilute colloidal suspensions. Stabilization of colloidal particles (e.g., clay minerals, polystyrene latex (PSL) particles, and fullerene C_{60} NPs) by organic anions, due to steric and electrostatic interactions, can lead to increased repulsion between uniformly and negatively charged particles (Chen and Elimelech, 2007; Tombacz et al., 1999; Walker and Bob, 2001). Mylon et al. (2004) reported that natural organic matter (NOM) macromolecules adsorbed on colloids could enhance hematite colloid stability. Illés and Tombácz (2006) found that humate-coated magnetite NPs formed stable colloidal suspension, which prevented particle aggregation or sedimentation over a wide range of solution pH. Humic substances with abundant carboxylic (–COOH, $–COO^-$) and phenolic (–OH) functional groups can exist as negatively charged polyelectrolytes. The interaction of these functional groups with surface active sites of NPs results in the adsorption of humic substances, which can modify the surface charge status of the NPs. Electrostatic attractive forces, ligand exchange, and cation bridging have all been reported as possible mechanisms responsible for NOM adsorption on colloidal particles (Elfarissi et al., 1998; Illés and Tombácz, 2006; Kretzschmar et al., 1998; Tombacz et al., 1999). Cationic polymers have also been found to facilitate adsorption of humic acid as coatings on the surfaces of iron oxide particles (Kim and Walker, 2001).

Magnetite NPs have recently attracted widespread attention because of their unique properties, including high surface-to-volume ratio, high chemical reactivity, the nearly full polarization, and supermagnetisim (Latham and Williams, 2008; Majewski and Thierry, 2007; Teja and Koh, 2009; Zhang et al., 2007). Due to the magnetic dipole–dipole interactions a substantial attractive force can exist among the magnetite NPs in addition to the classic DLVO forces (e.g., electrostatic repulsion and van der Waals). To achieve big enough repulsive forces (electrostatic repulsion and steric repulsion) to counter the magnetic attraction, surfactants with polymer structure or macromolecules are commonly employed as the dispersants to keep magnetite suspension stable. In this study, TMAH (tetramethylammonium hydroxide pentahydrate) was used for this purpose. The objective of this study was to quantify the aggregation behavior and kinetics of magnetite NPs over a wide range of pH and ionic strength, in the presence of different concentrations of dissolved NOM. A large number of batch experiments were conducted to measure the hydrodynamic size of magnetite NPs via dynamic light scattering under a variety of experimental conditions. Aggregation rate, stability ratio, and *CCC* were calculated to quantify experimental results and the DLVO theory was employed to evaluate the observed behaviors. In addition, atomic force microscope (AFM) was used to provide direct visual observations of interactions of HA and Fe_3O_4 particles, which provided confirmation of the observed HA effects on NP aggregation.

2. Materials and experimental methods

2.1. Synthesis and characterization of magnetite NPs

Magnetite NPs were selected as model NPs in this study to represent the category of reactive metal oxides NPs. The magnetite NPs were synthesized using a co-precipitation method. The starting solution was prepared by mixing 4 mL of 0.5 M $FeCl_3 \cdot 6H_2O$ (Sigma-Aldrich) and 1 mL of 1 M $FeCl_2 \cdot 4H_2O$ (Sigma-Aldrich). Magnetite precipitated when 25 mL of 0.7 M NH_4OH (Fisher Scientific Inc., NJ) was added into the solution at room temperature (25 °C) while mixed with strong magnetic stirring. After complete co-precipitation, the produced magnetite particles were attracted using NdFeB permanent magnet placed under the reaction beaker for collection. The particles were washed 3 times with deionized water (DI) and then dispersed into10 mL (0.028 g/mL) tetramethylammonium hydroxide pentahydrate (TMAH, Sigma-Aldrich) solution following dilution with DI water to a total volume of 30 mL.

A dynamic light scattering (DLS) particle sizer (Zetasizer ZEN3600) was used to measure the hydrodynamic diameter of the prepared magnetite NPs, which gave an average value of 58.0 ± 0.3 nm. The structure and morphology of the particles were studied using Philips X-Pert X-ray diffractometer (XRD) with Cu Kα radiation (λ = 1.5405 A) and transmission electron microscope (TEM, JEOL JEM-3010). The magnetic property was measured by a Lakeshore vibrating sample magnetometer (VSM) at room temperature.

2.2. Humic acid preparation

Humic acid (HA) suspension was prepared by dissolving 0.1 g Elliott soil humic acid standard (1S102H) (H_2O: 8.2%; Ash: 0.88%; C: 58.13%; H: 3.68%; O: 34.08%; N: 4.14%; S: 0.44%; and P: 0.24%), purchased from the International Humic Substances Society (IHSS), into 500 mL DI water and was stir-mixed for 1 week. Subsequently, the suspension was filtered through 0.45 μm membrane filter, and the pH of the filtrate was adjusted from 3.4 to 6.7. The HA stock was stored in the dark at 4 °C. The organic matter (OM) content of the stock solution was measured to be 40 mg L^{-1} via UV–VIS measurement based on a known dissolved mass concentration. The stock was diluted to 2–20 mg L^{-1} for use in the aggregation experiments.

2.3. Aggregation kinetic experiments

In this study, pH- and ionic strength-dependent aggregations of magnetite NPs in the absence and presence of HA were measured over a wide range of pH (3–10) and ionic strength (1–100 mM). Aggregation kinetics was determined by time-resolved dynamic light scattering measurements (Zetasizer, ZEN 3600, Malvern Instruments Ltd.). For each aggregation experiment in the absence of HA, NaCl solution was adjusted to desired pH and ionic strength first, and then a predetermined amount of concentrated magnetite NP stock (7600 mg L^{-1}) was introduced to obtain particle concentration of 25 mg L^{-1}. After addition of NPs, the suspension was quickly shaken and then 1.5 mL of the well-mixed suspension was transferred into a cuvette for hydrodynamic size measurements. Each sample was measured over a time period of 15–20 min with a 20-s time interval between each measurement. The estimated time gap between when

the aggregation began and data collection was ~30 s. For each experiment in the presence of HA, a predetermined amount of HA stock was introduced to a pH and ionic strength-adjusted electrolyte solution (buffer solution was employed) before adding the NPs. HA concentration was controlled at 2, 3, 5, 10, and 20 mg L^{-1}, respectively, for different sets of experiments. After mixing the HA and NPs, the pH and ionic strength of each sample were measured and pH was readjusted when necessary. Zeta potential values of the NPs at different pH and ionic strength were determined via electrophoresis mobility measurements at 25 °C using a Nano Zetasizer in the presence and absence of HA.

2.4. Atomic force microscope (AFM) observation

Atomic force microscope (AFM) is one of the most powerful tools for determining surface topography. Unlike X-ray crystallography and electron microscopy (EM), tapping-mode AFM allows biomolecules and micro/nano particles to be imaged in situ while biological processes or aqueous interactions are at work. Friction measurements by AFM can be used to characterize sample surface properties, which offer a great opportunity to determine not only sample size but also complex surface features (Meyer and Amer, 1990).

AFM experiments were preformed to directly observe NP aggregation behavior and to confirm results obtained from batch aggregation experiments. Selected experimental conditions under which the NP suspensions were imaged with AFM included acidic (pH 5) and alkaline (pH 8) pH as well as low (5 mM NaCl) and high (15 mM NaCl) ionic strength. The observations were performed both in the absence and presence of HA (2 mg L^{-1}).

Before each AFM observation session, fresh samples were prepared on-site following the same procedure as for batch aggregation experiments. All samples were ready 10 min prior to imaging to ensure that all the images were captured at a constant interaction time.

The AFM employed in this study was a Bioscope II atomic force microscope (Veeco Instruments Inc.), mounted on an Axiovert 200 inverted fluorescent microscope (Carl Zeiss Inc.). The tips were silicon nitride probes (Veeco Instruments Inc.) and had a nominal spring constant of 0.02 N/m. The images collected were in four forms: height, deflection error, friction, and Z sensor.

3. Theoretical considerations

3.1. Stability ratio and critical coagulation concentration

Time-resolved dynamic light scattering (DLS) is commonly used to investigate particle aggregation kinetics (Holthoff et al., 1996). Hydrodynamic radius (R_h) as a function of time (t) is obtained from DLS measurements. The initial rate of change of R_h is proportional to kn_0, which can be written as (Schudel et al., 1997; Mylon et al., 2004):

$$\left(\frac{dR_h}{dt}\right)_{t\to 0} \propto kn_0 \tag{1}$$

where k is aggregation rate constant, n_0 is initial particle number concentration. The stability ratio (W) is defined as the ratio of the fast aggregation rate, k^f, to the slow aggregation rate, k^s. For suspensions with the same particle concentrations in both fast aggregation regime and slow aggregation regime, W can be expressed as:

$$W = \frac{k^f}{k^s} = \frac{\left(\frac{dR_h}{dt}\right)^f_{t\to 0}}{\left(\frac{dR_h}{dt}\right)^s_{t\to 0}} \tag{2}$$

Based on the initial slope of the R_h–t curve determined in actual aggregation experiments, the stability ratio W can be obtained without having to determine the absolute aggregation rates. Plotting W as a function of solution ionic strength and extrapolating the curve gives the minimum concentration at which fast aggregation occurs and at this stage, particle size increases independent of electrolyte concentration. This concentration is defined as the critical coagulation concentration (*CCC*). Please note that there was a 30-s time gap between the on-site of initial aggregation and reading of particle size by the Zetasizer, which was needed to adjust the pH and allow stabilization of the instrument between measurements. Because we know that the initial particle size was 58 nm (R_h = 29 nm) at time 0, we included this point when estimating the initial slopes of the R_h–t curves. Thus, for the estimation of k^f, the first 70 s (0 to 70 s) was treated as the initial aggregation stage that included somewhat limited number of data points (total of 3). Because aggregation tends to happen very quickly at the initial stage, this could have caused some error in the estimation of "true" R_h values. However, the errors were not significant (with R^2 values ranging from 0.72 to 0.87) and should not affect meaningful comparison of W and *CCC* between treatments.

3.2. DLVO particle–particle interaction energy

The DLVO (Derjaguin and Landau, 1941; Verwey and Overbeek, 1948) theory is employed in this study to explain the aggregation behaviors of magnetite NPs under various aqueous conditions. The DLVO total interaction energy is determined by the sum of van der Waals attractive (V_A) and electric double layer repulsive (V_R) forces that exist between particles as they undergo Brownian motion (Elimelech et al., 1995):

$$V_T = V_{vdw} + V_{el} \tag{3}$$

The van der Waals attractive energy and electrical double layer repulsive energy are expressed as the following:

$$V_{vdw} = \frac{-A}{6}\left[\frac{2a^2}{s(4a+s)} + \frac{2a^2}{(2a+s)^2} + \ln\frac{s(4a+s)}{(2a+s)^2}\right] \tag{4}$$

$$V_{el} = 2\pi\varepsilon a\delta^2 \ln\left[1 + e^{-ks}\right] \tag{5}$$

where A (J) is the Hamaker constant, a (m) is the radius of particles, s (m) is the distance between surfaces of two interacting particles, $\varepsilon = \varepsilon_r\varepsilon_0$ is the dielectric constant where ε_r (78.54), for water at 298 K, is the relative dielectric constant of the medium and ε_0 (8.85×10^{-12} C^2 J^{-1} m^{-1}) is the permittivity in vacuum, ζ, the zeta potential of the charged particles, is assumed to equal the surface potential (Elimelech et al., 1995), k (m^{-1}) is the reciprocal of the thickness of the double layer and $k = 2.32\times10^9$ $(\Sigma C_i Z_i^2)^{1/2}$ where C_i is the concentration of ion i and Z_i is its valency value.

3.3. Hamaker constant determination

Hamaker constant (A), which characterizes the van der Waals interaction between two colloidal particles in a liquid medium, depends on particle surface geometry and composition, and the type of medium (Bergstrom et al., 1999). Different values of the Hamaker constants for magnetic substances such as Fe, Fe_2O_3, and Fe_3O_4 have been reported in the literature. The Hamaker constant values found in the literature range from ~10^{-19} J (Phenrat et al., 2007; Sander et al., 2004; Sverjensky and Sahai, 1998; Zhang et al., 2007) to ~1–10×10^{-20} J (Anastassakis, 2002; Berka and Rice, 2004; He et al., 2008; Schudel et al., 1997). For magnetic particles with surfactant (or NOM) surface coating, in addition to the attractive van der Waals (V_{vdw}) interaction, the total attraction potential should also take into account magnetic (V_m) attraction and steric repulsion (V_{ster}). In this case, the classic DLVO theory has been extended

to include magnetic attraction (Phenrat et al., 2007; Zhang et al., 2007). Quantification of the interaction energy using DLVO is believed to be more accurate when an experimentally determined Hamaker constant is employed in the calculation. Because the engineered magnetite NPs used were dispersed in a TMAH surfactant solution, which may induce unique medium properties, it is crucial to experimentally determine a Hamaker constant for the specific experimental conditions used in this study rather than selecting a literature value. Therefore, experimental results were fitted to the conventional DLVO equation to obtain the Hamaker constant, which represents an effective (or apparent) value that has incorporated the interparticle magnetic effect and steric stabilization effect.

Based on the DLVO theory, there is no energy barrier present between interacting particles at the *CCC* where the electric double layer repulsive interaction equals the van der Waals attractive interaction. Therefore, the experimental *CCC* values determined for a series of types of NaCl solutions (without and with HA of different concentrations) were used to calculate Hamaker constants for magnetite NPs. This method is similar to that reported in the literature (Amal et al., 1990; Mylon et al., 2004).

The surface force components have been employed to estimate surface free energy of a solid (Vanoss et al., 1988; Vanoss et al., 1989). In many studies, the Lifshitz–van der Waals component (LW) is taken to represent the dispersion component. To obtain the Lifshitz–van der Waals components for both NP and HA suspensions, the fitted Hamaker constant, surface free energy components (Plaza et al., 2002), and Lifshitz–van der Waals surface tension (Brown and Jaffe, 2006) were taken into account.

The Hamaker constant for two identical particles interacting through a liquid medium can be calculated from the following expression (Chen and Elimelech, 2007):

$$A_{pwp} = \left(\sqrt{A_{pp}} - \sqrt{A_{ww}}\right)^2 \tag{6}$$

where A_{ii} is the Hamaker constant of material i (i = p, w) and the subscripts p and w stand for particle and water, respectively. Using the apparent A value estimated from fitting experimental data to the DLVO equation (Eq. (6)), as described previously, A_{pp} in vacuum is obtained.

According to the Lifshitz–van der Waals surface tension, A_{pp} and A_{pwp} can be written as:

$$A_{pp} = 24\pi l_0^2 \gamma_p^{LW} \tag{7}$$

$$A_{pwp} = 24\pi l_0^2 \left(\sqrt{\gamma_p^{LW}} - \sqrt{\gamma_w^{LW}}\right)^2 \tag{8}$$

where l_0 is the equilibrium separation distance between the surfaces of two interacting particles, and usually it is taken as 1.58 ± 0.08 Å (Vanoss, 1994), and γ_x^{LW} is the Lifshitz–van der Waals component of the surface free energy of the particle ($x = p$) or the water/humic acid solution ($x = w$).

The fitted Hamaker constant, A_{pwp} was then used to calculate, with Eqs. (6) and (7), γ_p^{LW} for magnetite NPs. Concerning the effect of HA adsorption, Ramos-Tejada et al. (2003) found that the values of γ^{LW} and γ_p^{LW} for iron particles did not vary significantly with addition of humic acid over a wide range of solution pH and HA concentrations (0 to 200 mg L^{-1}). Therefore, the assumption that $\gamma_{p\,(HA)}^{LW} = \gamma_{p\,(bare)}^{LW}$ was used in Eq. (8) to obtain γ_{HA}^{LW} for the humic acid system. Using the DLVO-fitted $A_{pwp,water}$ (5.2×10^{-20} J) and a known $A_{ww,water}$ value (3.7×10^{-20} J), the $A_{pp,vacuum}$ was calculated (Eq. (6)) to be 1.76×10^{-19} J. The $\gamma_{p,bare}^{LW}$ was obtained as 93.83 mJ m^{-2} (Eq. (7)) and γ_{HA}^{LW} as 25.77 mJ m^{-2} (Eq. (8)) at 2 mg L^{-1} HA. Compared with γ_{water}^{LW} (21.8 mJ m^{-2}), γ_{HA}^{LW} (25.77 mJ m^{-2}) is slightly higher, which resulted in a smaller Hamaker constant for magnetite NPs in the presence of H. Using the same method, the Hamaker constants were obtained for the systems with higher HA concentrations. Compared to the value of 4×10^{-20} J at 2 mg L^{-1} HA, the Hamaker constants at 3 mg L^{-1}, 5 mg L^{-1} and 10 mg L^{-1} HA were calculated to be 1.98×10^{-20} J, 1.52×10^{-20} J and 1.38×10^{-20} J, respectively, showing a decreasing trend with increasing HA concentration.

4. Results and discussion

4.1. Properties of magnetite NPs

The XRD pattern of as-prepared particles confirms that the particles are face centered cubic (fcc) magnetite. The average size of the particles was estimated to be 12.2 ± 1.2 nm by Scherer's equation (Cullity, 1978; Wan et al., 2006). Fig. 1 shows a typical TEM graph of the as-prepared magnetite particles and a TEM associated electron diffraction pattern, which shows the same fcc structure as observed by XRD.

The magnetite NPs were stabilized by adding a surfactant (tetramethylammonium hydroxide, $(CH_3)_4NOH$, or TMAH) at a concentration of 0.0093 g mL^{-1}. Surfactant molecules adhere to the surface of magnetite particles and coat the particles with hydroxide anions, which attract tetramethylammonium cations, forming a diffuse shell around each particle and creating repulsion between the particles.

From DLS measurements, the average hydrodynamic diameter of the magnetite NPs (Z_{avg}) was determined as 58 ± 0.02 nm. As TMAH releases hydroxide anions into the aqueous solution, the original pH of the magnetite suspension was high at 12.8 ± 0.2. For batch aggregation experiments, the original high pH stock solution was diluted 300 times resulting in a diluted concentration of 25 mg L^{-1}, which had a pH of 9.8 ± 0.2. The zeta potential measured for this diluted suspension was -34.1 ± 0.4 mV.

4.2. Effect of HA on magnetite NPs surface charge

The negative zeta potential (ZP) of −34.1 mV indicates that magnetite NPs carry a net negative charge at the original pH of 9.8. The ZP value changed with changing solution pH and ionic strength, and the change was affected by the presence of HA, as shown in Fig. 2.

In Fig. 2a, ZP values are plotted as a function of pH, ranging from 3 to 10 in 1 mM NaCl electrolyte solution, in the absence and presence of HA at 5 different concentrations. The pH at which ZP = 0 is 7.1 in the absence of HA, which by definition is taken as the point of zero charge (PZC). This value is within the range of PZC values (6.8 to 8.1) as reported in the literature for magnetite in NaCl buffer solutions (Illés and Tombácz, 2006; Regazzoni et al., 1983; Tombacz et al., 2004). Different synthesis procedure, aqueous medium conditions, and measuring methods are likely the cause for the different PZCs as reported in the literature.

In the presence of HA, the entire ZP curve shifted downward, resulting in lower PZCs (pH 5.8 for 2 mg L^{-1} HA and pH 3.77 for 3 mg L^{-1} HA). The observed shifts are likely caused by adsorption of HA on magnetite particles, which changed their surface charge. Humic substances carry many functional groups, including major species such as carboxylic (–COOH) and phenolic (–OH). These highly reactive polar groups tend to bound with the active groups on metal oxide surfaces, which alter particle surface charge (Sander et al., 2004; Tombacz et al., 2004). Fig. 2a shows that with 2 mg L^{-1} HA and 3 mg L^{-1} HA at pHs lower than the PZC, negatively charged HA neutralizes the positive charges on magnetite particles, reducing ZP. Comparison of the ZP curves at no HA and 2 mg L^{-1} indicates that this effect is more significant at pHs close to the PZC value (e.g. pH 6 and 7) but diminishes as pH decreases. This is because the limited amount of HA can only neutralize a fraction of the large amount of H^+ covering

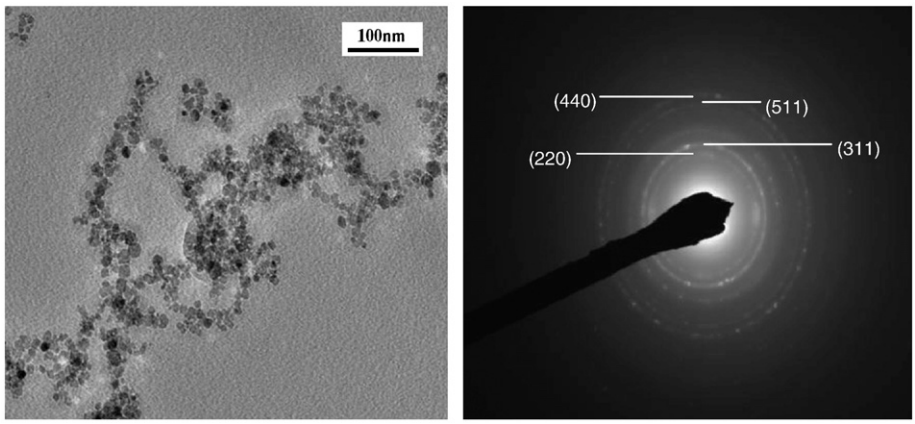

Fig. 1. TEM graph and TEM associated electron diffraction pattern of as-prepared magnetite NPs.

the particle surfaces at low pH. Moreover, decreased ionization of HA with decreasing pH may have also contributed to reducing the ability of HA to neutralize H^+ ions on NPs surfaces. The ZP curve shifted even more as the HA concentration was increased to 3 mg L^{-1}. With this small increase of HA, significantly more positive charges on NPs surface were neutralized hence a dramatic decreasing PZC was observed (pH 3.77). When HA concentration was increased further (from 4 to 20 mg L^{-1}), the ZP values stayed in the negative regime and are more negative with the increasing HA concentration.

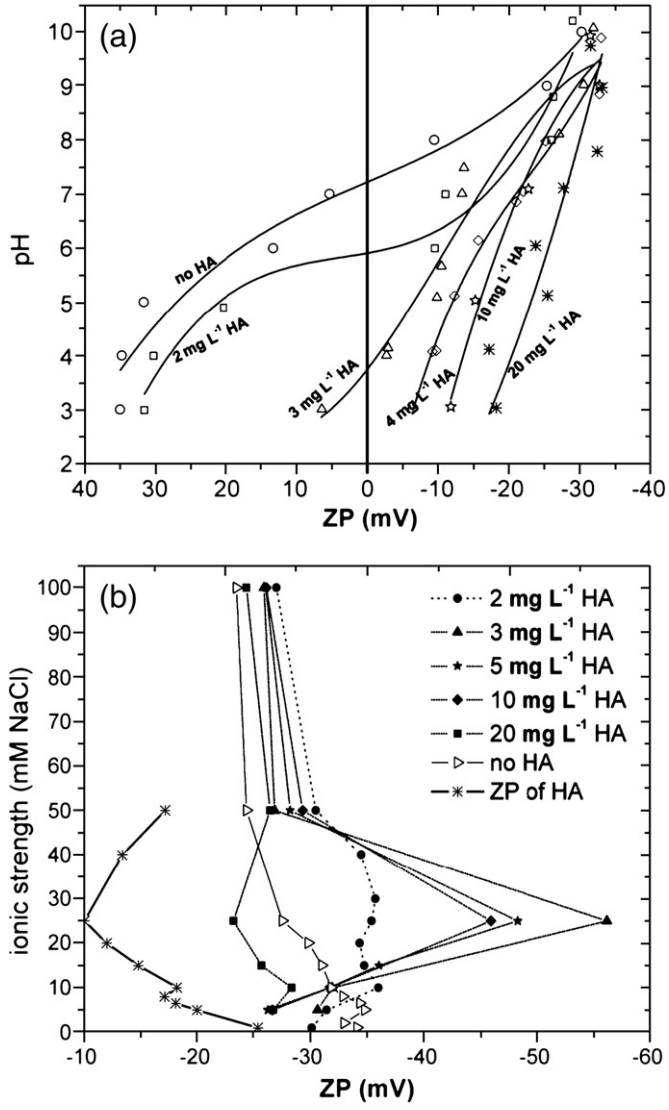

Fig. 2. Effect of HA on zeta potential (mV) of magnetite NPs (a) as a function of pH in 1 mM NaCl solution (the solid and dash lines show the trend of ZP change, fitted with 3-order polynomial regression) and (b) as a function of ionic strength at pH 9.8 (the cross symbols show the ZP profile of HA).

At pHs greater than the PZC (i.e. pH 5.8 at 2 mg L^{-1} HA), because both magnetite NPs and humic polyanions are negatively charged, adsorption of HA on the particles is in general not expected. However, in this study, the interaction between magnetite particles and HA was likely complicated by the presence of trace levels of the TMAH surfactant, the dispersion agent that could act as a cationic polymer addictive. It has been reported that polymer additives could improve the adsorption of humic acid under apparently unfavorable conditions (Kim and Walker, 2001; Lurie and Rebhun, 1997). In our experiments, TMAH polymer likely promoted the adsorption of HA onto the surfaces of magnetite particles. In addition, the specific (non-Coulombic) attraction between HA and magnetite particles might also be present, which could induce a substantial sorption of HA onto the NPs surfaces (Vermeer et al., 1998). For these two reasons, at high pH, binding/coating of the negatively charged HA on the particles made them more negative, hence, the more negative ZP values measured in the presence of HA. Similar results have been reported by Illés and Tombácz (2006).

Fig. 2b shows the effect of HA on the surface charge of magnetite NPs as a function of ionic strength at pH 9.8. In the absence of HA, ZP of magnetite NPs decreased (i.e., became less negative) with the increase of ionic strength due to electric double layer compression. In the presence of HA, more negative ZP values at ionic strength below 25 mM NaCl and an decreasing ZP (less negative) at ionic strength above 25 mM NaCl were observed, respectively, except that for HA of 20 mg L^{-1}. The general increasing ZPs (ionic strength below 25 mM NaCl) could be explained by the counter effects, due to addition of HA, of introduction of more negative charges, which makes ZP more negative, and double layer compression, which makes ZP less negative. The effects of HA on the surface charge of colloidal particles as a function of ionic strength have been reported elsewhere (Mylon et al., 2004; Ramos-Tejada et al., 2003; Verrall et al., 1999). In Mylon et al.'s work, the SRHA-coated hematite colloids showed a more negative zeta potential than the bare particles with the same solution pH as a result of the negative charges brought by HA coating. This is in agreement with our finding with magnetite NPs at high ionic strength range in this study (except for 20 mg L^{-1} HA). Ramos-Tejada (2003) examined the electrophoretic mobility of hematite particles with an increasing $NaNO_3$ ionic strength in presence of HA and found at higher Na^+ concentration the mobility was not affected much, which indicates that zeta potential of the particles was essentially independent of ionic strength at high ionic strength values. This result is also consistent with the findings in this study.

The discrepancy of ZP behavior at 20 mg L^{-1} HA could be explained considering the zeta potential profile of HA's own. It is likely that the HA at high enough concentration could take over in terms of charge status of magnetite NPs. Fig. 2b also shows the ZP profile of HA macromolecules as a function of ionic strength, which reveals a very similar trend to that of magnetite NP in presence of 20 mg L^{-1} HA. As the critical concentration of HA for complete neutralization of the NPs surface charge was found between 3 mg L^{-1} and 4 mg L^{-1} (>2 mg L^{-1}, Fig. 2a), it is understandable that the magnetite NPs have a different ZP status at 2 mg L^{-1} HA compared to that at 3–10 mg L^{-1} HA (Fig. 2b).

Moreover, the surface charge status of magnetite NPs in the presence of HA (2 mg L^{-1}–10 mg L^{-1}) exhibited a very special characteristic at 25 mM NaCl where the ZPs increased dramatically. This distinct behavior could be understood employing the preferential adsorption model theory (Zukoski and Saville, 1986) and the hairy layer model theory (Elimelech and O'Melia, 1990). The preferential adsorption model suggests that the adsorption of anions onto negatively charged particle surfaces may cause a more negative electrokinetic potential. This preferential sorption could be attributed to the less hydration of anions compared to cations. This would allow the anions to get closer to the particle surface and therefore lead to an increasing surface potential. The hairy layer model assumes that a layer with special chain-like structure on particle surfaces is responsible for the maximum values of surface potential. With the increase of ionic strength, the repulsion among the negatively charged surface groups is enhanced. As this hairy surface layer consequently is shrinked, the plate of shear in the electrostatic double layer moves inward, causing an increasing ζ potential. In this study, especially in the presence of HA and TMAH surface coating, both the preferential adsorption model and hairy layer model are applicable as possible explanations for the maximum ZP values observed at 25 mM NaCl. A similar trend was also observed in Pelley and Tufenkji's (2008) where they reported that the measured ZP reached a maximum value at certain ionic strength (i.e., 10 and 3 mM KCl, respectively, for 1500 nm and 110 nm latex particles) instead of a continuous decrease with the increase of ionic strength. In this study, the maximum ZP value followed a decreasing trend from 3 mg L^{-1} to 10 mg L^{-1} HA at 25 mM NaCl, which is attributed to the increasingly overwhelming effect of HA coating with the increase of HA concentration.

4.3. Effect of HA on aggregation of magnetite nanoparticles

Based on the understanding of HA's ability to modify particle surface charge as discussed above, the impact of HA on magnetite NPs aggregation as functions of solution pH and ionic strength was evaluated. Fig. 3 shows results from a series of early stage aggregation experiments measuring hydrodynamic sizes as a function of time by DLS over a wide range of solution pH and ionic strength in the presence and absence of HA.

Fig. 3a shows that in the absence of HA, suspensions of magnetite NPs were not stable at pHs from 6 to 8, and the measured average hydrodynamic sizes of magnetite aggregates increased continuously and quickly with time, an indication that aggregation occurred rapidly. At the PZC (7.1), the net particle surface charge reduces to zero and fast aggregation takes place when the interparticle interaction is the greatest (minimum repulsion). This explains the observed aggregation behavior of magnetite particles when suspension pH is close to the PZC (e.g., at pH 6, 7, and 8), for example, the greatest aggregation was observed at pH 7 (shown in the insert of Fig. 3a). At pHs 3 to 5 and 9 to 10, which are far from the PZC, magnetite suspensions remained stable and the average particle size remained similar to the original size (60 nm).

Magnetite NP aggregation as a function of pH in the presence of various concentrations of HA is illustrated in Fig. 3b–e. As expected, the aggregation behavior is controlled by the surface charge status of the particles under the different conditions examined and corresponds well with the measured shifts of PZC values at the different HA concentrations. Because adsorption of HA caused the decrease in the PZC of magnetite NPs from 7.1 to 5.8 at 2 mg L^{-1} HA and to 3.77 at 3 mg L^{-1} HA, aggregation was observed to occur at a lower pH of 5 (Fig. 3b) and 4 (Fig. 3c) compared to pH 6 in the absence of HA. When the HA concentration was increased to 4 mg L^{-1}, aggregation only occurred at pH 3. Further increase to 10 mg L^{-1} HA, no aggregation was observed over the range of pH 3–10. Overall, HA can both enhance the aggregation and stabilize the suspension of magnetite NPs depending on the specific pH condition. This is consistent with the previous analysis on the effect of HA adsorption of surface charge status of magnetite NPs. Generally, in presence of low level HA (2 mg L^{-1} and 3 mg L^{-1}) at low pHs, HA neutralized the positive charges of the magnetite NPs resulting in reduced repulsive forces between the particles hence more aggregation (i.e. at pH 5 in the presence of 2 mg L^{-1} HA and at pH 4 in the presence of 3 mg L^{-1} HA). At higher pHs, HA brought more negative charges to particle surfaces therefore resulted in stronger electrostatic repulsion between the particles and therefore more stable suspensions (i.e. at pH 8 for 2 mg L^{-1} HA and at pH 5 for 3 mg L^{-1} HA). In the presence of higher level HA (4 mg L^{-1} and 10 mg L^{-1}), a more complete HA coating on NP particles led to a much stronger interparticle electrostatic repulsion and therefore a much more stable suspension was observed (Fig. 3d, e).

Fig. 4 shows aggregation of magnetite particles as a function of ionic strength in the absence (Fig. 4a) and presence (Fig. 4b) of HA during both slow and fast aggregation regimes. With increasing NaCl concentration, the rate of aggregation increased, corresponding to the so-called slow aggregation regime. At ionic strength higher than 25 mM NaCl (without HA, Fig. 4a) or 50 mM NaCl (with 2 mg L^{-1} HA, Fig. 4b), measured particle size was independent of electrolyte concentration and fast aggregation took place where aggregation was dominantly controlled by diffusion rather than interparticle interaction. The stabilizing effect of HA is indicated by the observed increase in the threshold ionic strength, at which fast aggregation regime began, from 25 mM in the absence of HA to 50 mM when HA was added (Fig. 4b).

The effect of HA concentration was investigated via conducting the aggregation experiments in the presence of 3, 10, and 20 mg L^{-1} HA over a range of ionic strength from 5 mM to 200 mM NaCl. Fig. 4c presents a set of sample measurements at 50 mM NaCl showing the increased stabilizing effect of increasing concentrations of HA at different concentrations on the magnetite NPs suspension. Greater interparticle electrostatic repulsion and steric stabilization are the two processes that together contributed to the stabilizing effect of HA at high pHs.

4.4. HA Effect on stability kinetics

The effect of HA on the stability of magnetite suspension is further supported by evaluating the stability ratio in the absence and presence of HA. The stability ratios (W) of magnetite NPs as a function of NaCl concentration in the absence and presence of HA were calculated using Eq. (2). The inverse values of W ($1/W$), also known as the attachment efficiency (α) defined as the probability of an irreversible attachment resulting from the collision of two colloidal particles, are plotted in Fig. 5. The ratio of k^s/k^f ($1/W$) is proportional to the ratio of slopes of the lines fitted to the R_h data, which was determined in both slow aggregation and fast aggregation (Chen et al., 2006). The $1/W$ profiles in Fig. 5 confirm the effect of ionic strength on NP stability, which decreases with increasing NaCl concentration until the slow aggregation rate k^s reaches the fast aggregation rate k^f. The intersection of the extrapolation through the fast and slow aggregation regimes yields the *CCC* values, which are 23.8 mM NaCl in the absence of HA and 41.7, 73.2, 108.6, and 125.5 mM NaCl in the

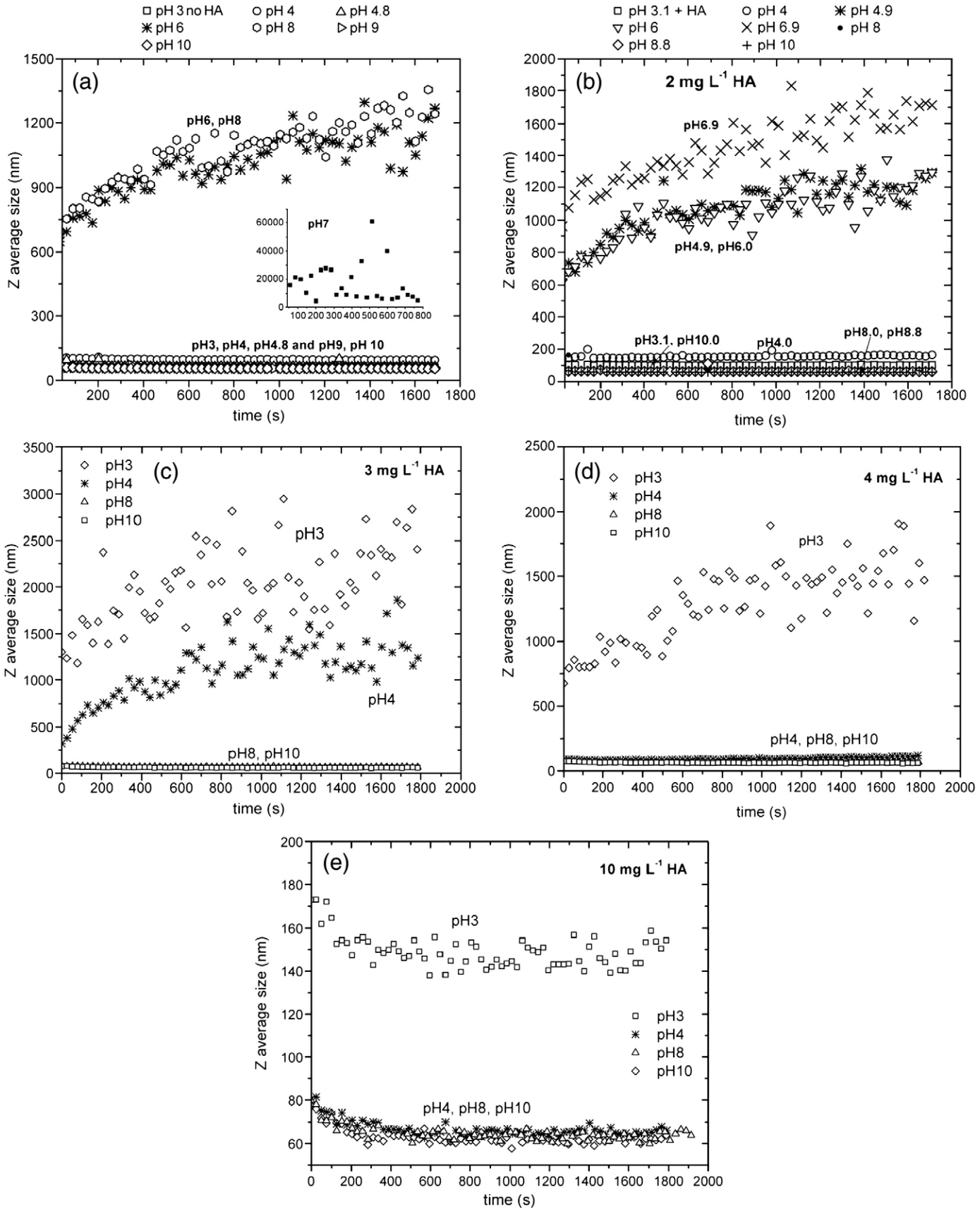

Fig. 3. Aggregation of magnetite NPs over a range of pH in the absence and at different concentrations of humic acid in 1 mM NaCl solution.

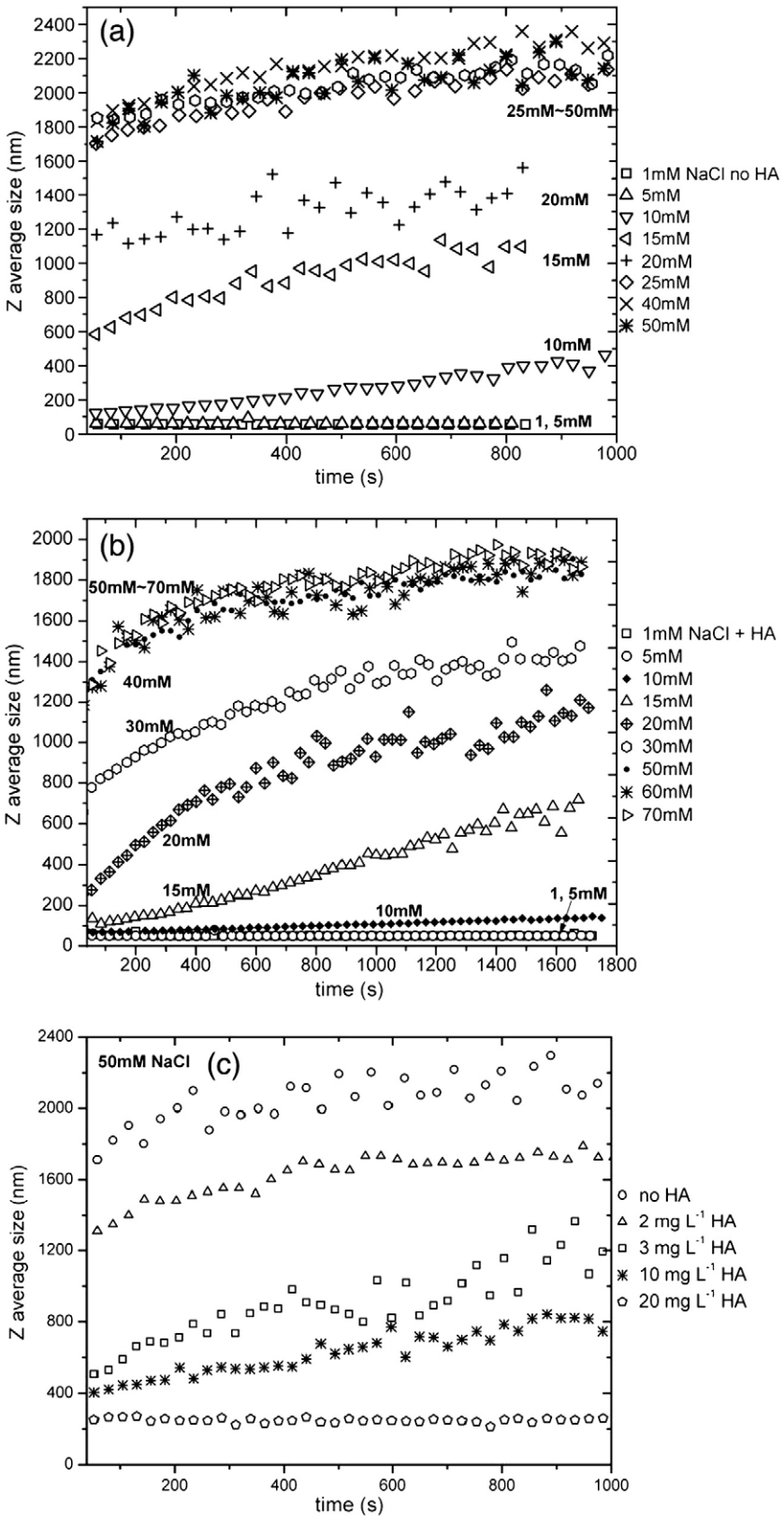

Fig. 4. Effect of humic acid on magnetite NP aggregation behavior at pH 9.8 over a range of solution ionicstrength: (a) no humic acid (b) with humic acid (2 mg L^{-1}); (c) with humic acid at various concentrations at 50 mM NaCl.

presence of 2, 3, 10, and 20 mg L^{-1} HA, respectively. When the k^s for HA system was normalized by k^f for no HA system ($k^s_{\text{with HA}}/k^f_{\text{no HA}}$), another $1/W$ profile (solid circle) was obtained (Fig. 5) (Chen and Elimelech, 2007). In the presence of HA (2 mg L^{-1}), the k^f was only 64% of that in the absence of HA, which indicates a slower increase of k^s in the HA system, i.e., the suspension is more stable. In other words, the attachment efficiency (i.e., formation of aggregates) in the presence of 2 mg L^{-1} HA was reduced to 64% compared to in the

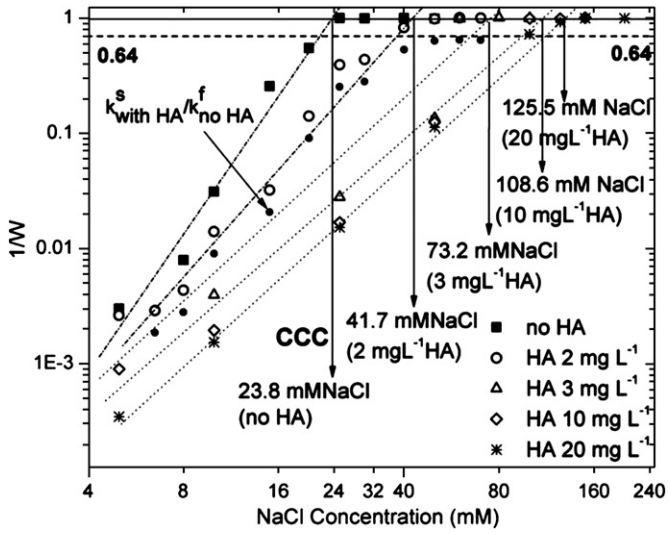

Fig. 5. Stability ratio and the *CCC* value of magnetite NPs as a function of NaCl concentration at pH 9.8 in absence (solid square) and presence (open symbols) of humic acid (2, 3, 10, and 20 mg L^{-1}). Use normalized aggregation rates ($k^s_{with\ HA}/k^f_{no\ HA}$), comparative stability ratios (solid circle) at 2 mg L^{-1} HA were obtained. The dashed lines are calculated extrapolations.

absence of HA. In addition to the resulted higher *CCC* values, increasing HA concentration also had an impact on the decreasing rate of the stability of magnetite NPs suspension. The suspension's stability decreased slower with increasing ionic strength due to more HA addition (Fig. 5).

4.5. DLVO evaluation of interactions between NPs

DLVO theory provides a useful tool for describing interparticle interactive energies of colloidal suspensions. We used the classic DLVO theory to model the interactions between magnetite NPs under different pH and ionic strength conditions in the presence and absence of HA. The fast and slow aggregations observed in the aggregation experiments have also been defined as diffusion-limited and reaction-limited aggregations, respectively. The stability profiles in Fig. 6 reveal these two aggregation regimes, which could be explained by the DLVO theory.

Plotted in Fig. 6 are the DLVO energy profiles for magnetite NP–NP interactions as a function of solution pH and ionic strength in the presence and absence of HA. As ionic strength increases, interparticle repulsion decreases reducing the energy barrier (Fig. 6a, b). At the critical coagulation concentration (*CCC*), diffusion-limited aggregation takes place because no repulsive force or energy barrier exists and the only factor controlling aggregation is Brownian diffusion.

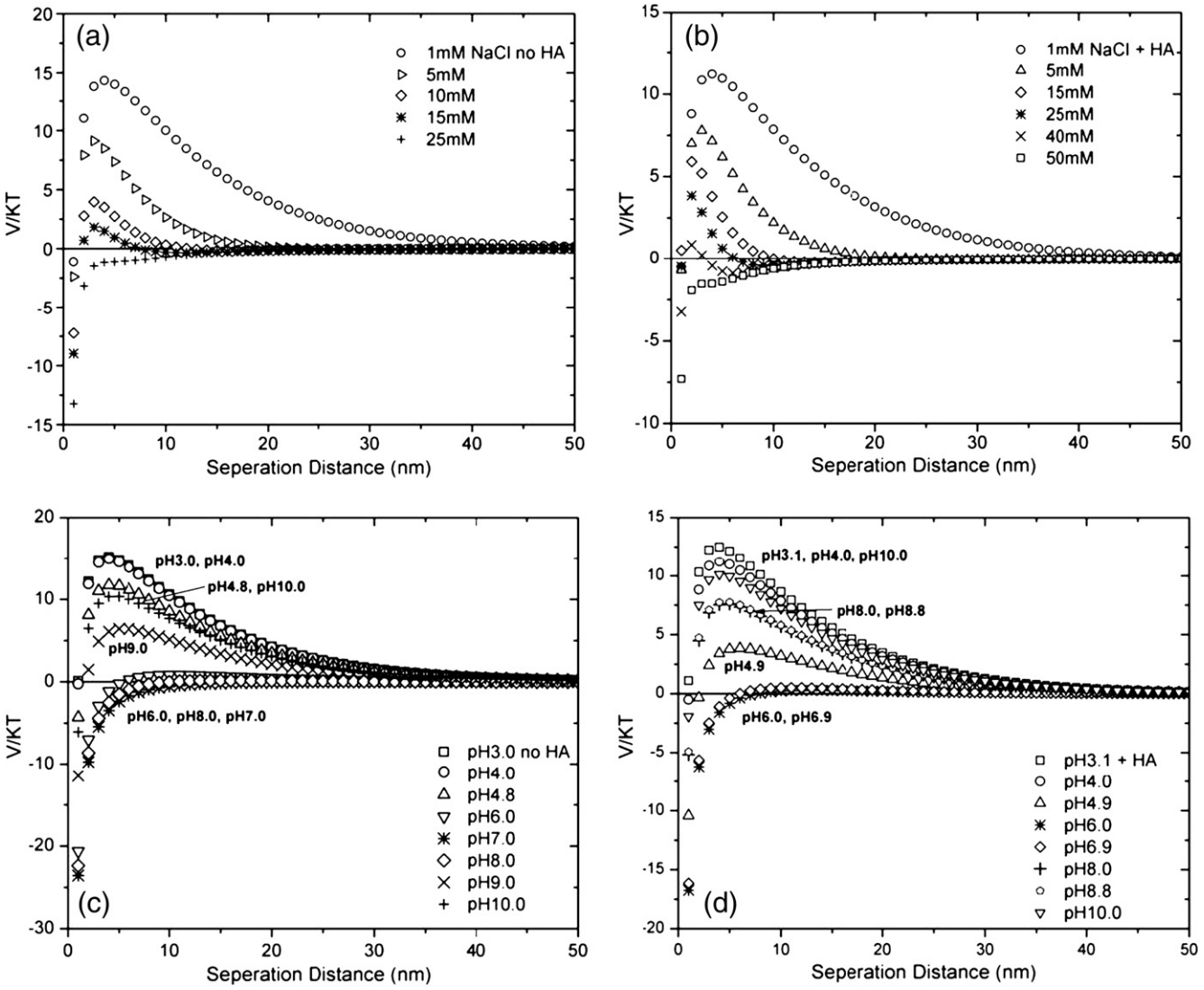

Fig. 6. DLVO interaction energy profiles for suspensions of magnetite NPs in the absence and presence of 2 mg L^{-1} HA, (a, b) as a function of ionic strength; (c, d) as a function of pH.

Fitting the experimental aggregation data to the DLVO energy curves through the calculated *CCC* values, Hamaker constant (*A*) was obtained, 5.2×10^{-20} J without HA and 4.0×10^{-20} J in the presence of 2 mg L^{-1} HA, respectively. Although the difference between the two values of *A* was not significant, in our case an obvious effect induced by this difference was observed in the subsequent DLVO calculations. The stability of magnetite particle suspensions in this study was apparently very sensitive to even a small change of *A*. The excellent agreement between the calculated energy curves with the experimental results at various pH values (Fig. 6c, d) indicates that the estimated *A* values were accurate.

DLVO calculations indicate that the energy barriers are comparatively lower at low pHs (pH 3, and 4) and low NaCl concentrations (1, and 2 mM) in the presence of HA than those in the absence of HA. This means increased likelihood for aggregation, which is consistent with the measured ZP values (Fig. 2). However, the addition of HA did not reduce stability of NPs under these conditions because the energy barriers were still big enough (above 10 V/KT) to maintain NP suspensions stable. When the pH is far from the PZC, DLVO theory predicts a high energy barrier, while when it is close to the PZC (Fig. 6c, d), the energy barrier reduces to below zero and fast aggregation occurs. The zero energy barriers occur and lead to a diffusion-limited aggregation when the NaCl concentration is at the *CCC* (Fig. 6a, b). The DLVO descriptions are consistent with ZP measurements (Fig. 2) and results from the aggregation experiments (Figs. 3 and 4).

To further examine how classic DLVO theory interpret the magnetite NP–NP interaction in presence of HA at higher concentrations, the interaction energy calculations were conducted for the 3 and 10 mg L^{-1} HA conditions using the fitted Hamaker constants, as previously described. As shown in Fig. 7, except for a slight underestimation of the energy barriers for 10 mg L^{-1} HA at pH 8 and 10 (Fig. 7d), the DLVO profiles well described the stability behaviors of magnetite NPs for higher HA concentrations as a function of pH (Fig. 3c, e). The secondary minima were found in the DLVO profiles at high ionic strengths (pH 10) (Figs. 6a, b and 7a, b), indicating a possibility that at these ionic strengths the magnetite NPs could form aggregates temporally in secondary minimum energy well. Upon elimination of the secondary energy minimum when ionic strength is reduced, they could deaggregate to become nano-scale particles again. The ionic strength corresponding to the occurrence of the secondary energy minimum was found to increase with the increase of HA concentration, i.e., 15 mM NaCl for no HA, 25 mM NaCl for 2 mg L^{-1} HA, 40 mM NaCl for 3 mg L^{-1} HA and 50 mM for 10 mg L^{-1}

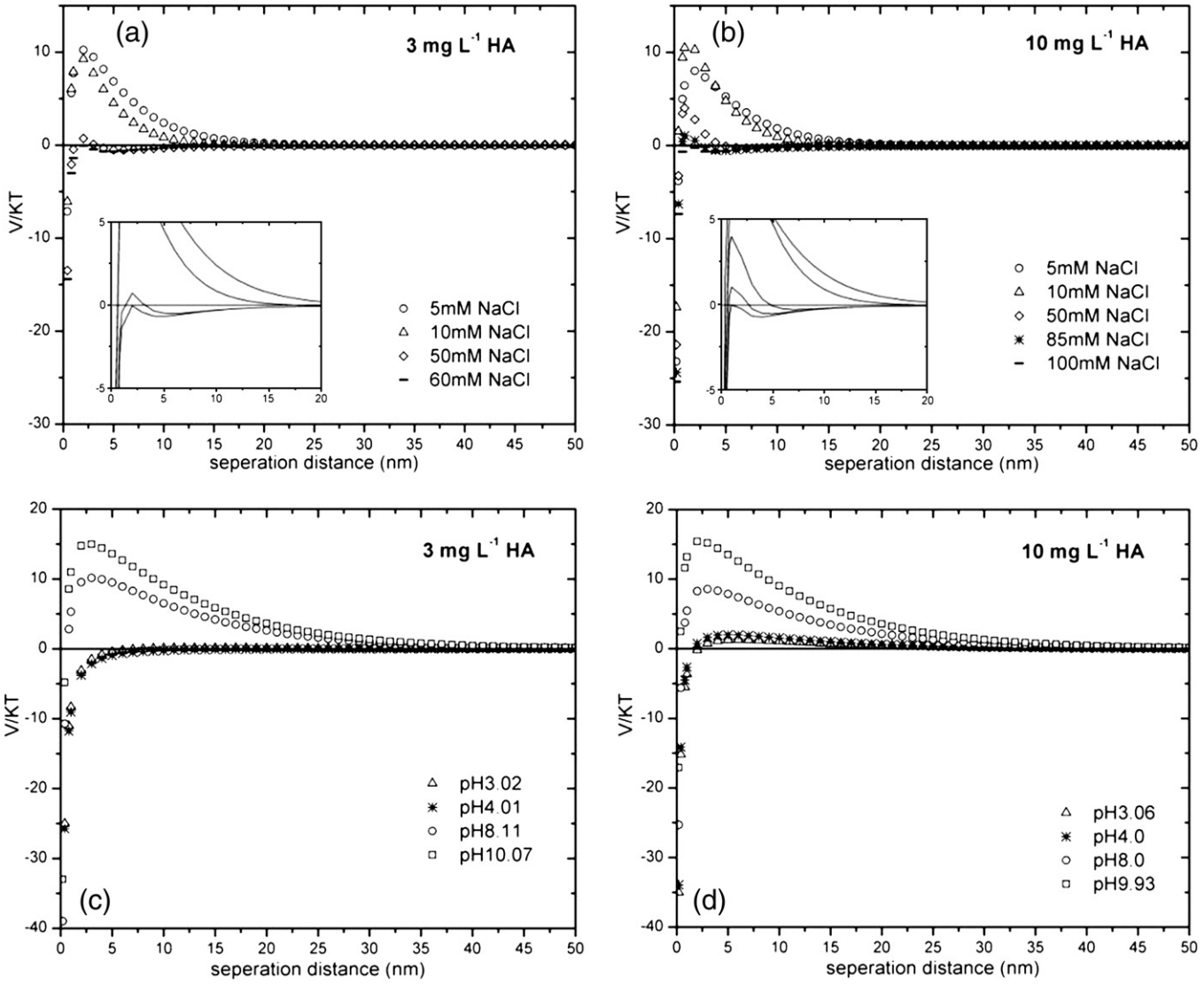

Fig. 7. DLVO interaction energy profiles for suspensions of magnetite NPs in the presence of HA (a 3 mg L^{-1}, b 10 mg L^{-1}) as a function of ionic strength; (c 3 mg L^{-1}, d 10 mg L^{-1}) as a function of pH. The insets in (a) and (b) highlight the major differences in the DLVO profiles for 3 mg L^{-1} HA and 10 mg L^{-1} HA.

HA. This suggests that in addition to increase the energy barrier, the presence of HA also helps to stabilize the magnetite NPs suspension by forming a secondary energy minimum at higher ionic strength.

4.6. AFM observations

Through AFM imaging, interactions of HA and magnetite particles and how such interactions affected particle aggregation were observed. AFM images of magnetite NPS in the absence (a) and presence (b) of HA as well as HA alone (c) in 5 mM NaCl solution are presented in Fig. 8. The average sizes of the particles in the images, estimated based on height measurements, are summarized in Table 1. At 15 mM ionic strength, magnetite NPs appear to be larger particles with an average size of 408 ± 3.1 nm (Fig. 9a, Table 1) without the presence of HA while with the addition of HA, the average size reduced to 121 ± 1.3 nm (Fig. 9b, Table 1). Interestingly, when viewing HA alone at pH 6.7, i.e., without magnetite NPs (Fig. 8c), they look like large "aggregates" having an average size of 400 ± 11.5 nm. However, when added into magnetite particle suspension, HA "aggregates" disappear and form bright yellow lines and circles around magnetite particles (Fig. 8b), indicating HA adsorption on particle surfaces. The HA "aggregates" completely disappeared in the presence of magnetite particles suggesting that these apparent "aggregates" observed in Fig. 8c were likely micelle-like structures, which disintegrated upon interaction with the magnetite particles. The real-time AFM images provide direct visual evidence on the role of HA, acting similarly to surfactants, in dispersing and stabilizing magnetite NP suspensions.

The stabilization effect of HA on aggregation of magnetite NPs is further demonstrated in Table 1 for different ionic strength and pH conditions. At a given pH of 9.8, HA slightly reduced the average particle size of magnetite at 5 mM but the effect was much more significant at higher ionic strengths of 15 and 25 mM. When solution ionic strength was maintained at 1 mM NaCl, addition of HA to magnetite particle suspension destabilized the suspension at pH 5, causing particle size to increase from 55 ± 2.7 nm to 360 ± 5.5 nm while at pH 8 the suspension was stabilized and particle size remained at $\sim 140 \pm 9.4$ nm, which is much smaller compared to the 325 ± 6.0 nm in the absence of HA. These AFM imaging results agree well with the aggregation results from the batch experiments, providing strong support for the NPs' stability kinetic findings.

Table 1
The effect of HA on the sizes of NPs measured via AFM image analysis under different ionic strength and pH conditions.

Solution conditions		NPs size (nm)	
		No HA	With HA
pH 9.8	5 mM NaCl	43 ± 0.7	36 ± 1.0
	15 mM NaCl	408 ± 3.1	121 ± 1.3
	25 mM NaCl	450 ± 7.4	218 ± 5.4
1 mM NaCl	pH 5	55 ± 2.7	360 ± 5.5
	pH 8	325 ± 6.0	140 ± 9.4

5. Conclusions

Through a series of aggregation kinetic experiments, this study demonstrates that the presence of HA can both stabilize and destabilize NP suspensions by altering the NP surface charge status, which is an important factor controlling the stability of NPs. Zeta potential measurements showed that the presence of HA led to a notable reduction of the PZC value of the magnetite NPs by either neutralize or increase, depending on solution pH and the loading of HA, the negative surface charge of magnetite NPs. The critical concentration of HA for complete particle surface charge neutralization was found to be around 3–4 mg L^{-1} for magnetite NPs. The observed aggregation behavior can be explained clearly via the analysis of NP surface charge status. Kinetic study on NP stability, showing a 36% decrease in attachment efficiency in the presence of 2 mg L^{-1} HA and increasing *CCC* values with the increase of HA loading, further quantified the stabilization potential of HA as function of ionic strength. DLVO energy calculations, using experimentally determined values of the Hamaker constant, provided consistent support to the experimental results. The concentration effect of HA was further proved via the observed changing of secondary minimum and energy barrier in DLVO profiles with the increase of HA introduction. Real-time AFM observations indicated that HA acted similarly to surfactant molecules where they could form micelles while in solution alone and then were absorbed onto magnetite surfaces upon mixing with the NP suspension as coatings, resulting in changes in particle surface charge hence their suspension stability. Results from this study clearly show that as natural organic matter (NOM), HA, even at a low concentration, can have a great impact on the stability and aggregation/deaggregation behavior of engineered magnetite NPs by changing particle surface charge status. These results have important implications on estimating the engineered magnetite NPs environmental hazards and understanding NPs environmental remediation functions in natural subsurface environments where NOM is in general abundant.

Acknowledgements

This work was supported in part, by the U.S. Environmental Protection Agency STAR Program (grant no R833318), and by the National Scientific Foundation of China (grant no 40525003 and no 40971247). We would like to acknowledge Dr. Elizabeth Adams (Delaware Biotechnology Institute, University of Delaware) for her assistance with AFM imaging. The first author also appreciates the financial support from the China Scholarship Council (CSC).

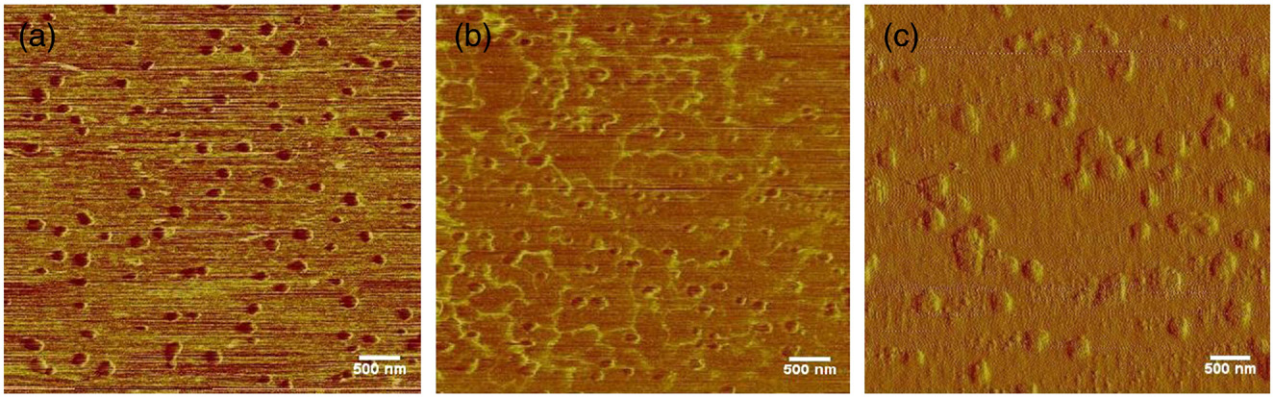

Fig. 8. AFM images of magnetite NPs in absence (a) and presence (b) of humic acid (2 mg L^{-1}) (pH 9.8), and (c) of HA alone (pH 6.7) in 5 mM NaCl solution.

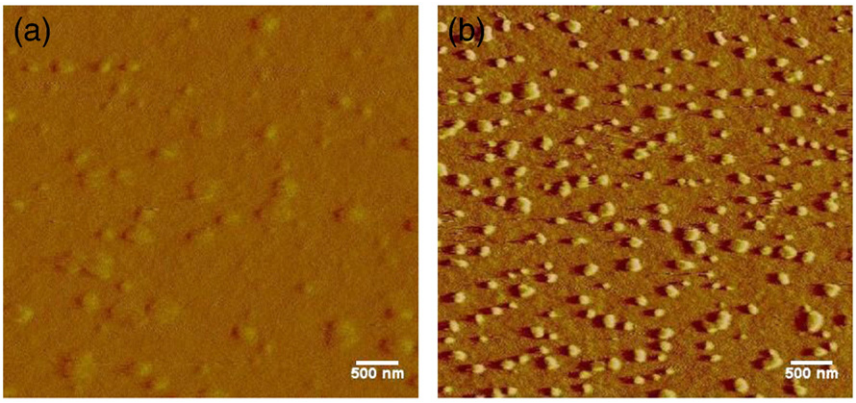

Fig. 9. The AFM images for magnetite NPs at 15 mM NaCl concentration in absence (a) and presence (b) of humic acid (2 mg L^{-1}).

References

Amal R, Coury JR, Raper JA, Walsh WP, Waite TD. Structure and kinetics of aggregating colloidal haematite. Colloids Surf 1990;46(1):1-19.

Anastassakis GN. Separation of fine mineral particles by selective magnetic coating. J Colloid Interface Sci 2002;256:114–20.

Bergstrom L, Blomberg E, Guldberg-Pedersen H. Interparticle forces and rheological properties of ceramic suspensions. Novel Synth Process Ceram 1999;159–1: 119–26.

Berka M, Rice JA. Absolute aggregation rate constants in aggregation of Kaolinite measured by simultaneous static and dynamic light scattering. Langmuir 2004;20: 6152–7.

Borkovec M, Behrens SH. Stabilization of aqueous colloidal dispersions: electrostatic and steric forces. Encycl Surf Colloid Sci 2006:5765–74.

Brown DG, Jaffe PR. Effects of nonionic surfactants on the cell surface hydrophobicity and apparent hamaker constant of a *Sphingomonas* sp. Environ Sci Technol 2006;40: 195–201.

Chen KL, Mylon SE, Elimelech M. Aggregation kinetics of alginate-coated hematite nanoparticles in monovalent and divalent electrolytes. Environ Sci Technol 2006;40(5):1516–23.

Chen KL, Elimelech M. Influence of humic acid on the aggregation kinetics of fullerene (C60) nanoparticles in monovalent and divalent electrolyte solutions. J Colloid Interface Sci 2007;309:126–34.

Christian P, Von der Kammer F, Baalousha M, Hofmann T. Nanoparticles: structure, properties, preparation and behaviour in environmental media. Ecotoxicology 2008;17:326–43.

Cullity BD. Elements of X-ray diffractions. Reading, MA: Addition Wesley; 1978.

Derjaguin BV, Landau L. Theory of stability of strongly charged lyophobic sols and of the adhesion of strongly charged particles in solutions of electrolytes. Acta Physicochim URSS 1941;14:633–62.

Elfarissi F, et al. Polyelectrolytic nature of humic substances aluminum ion complexes — interfacial characteristics and effects on colloid stability. Colloids Surf A Physicochem Eng Aspects 1998;131:281–94.

Elimelech M, Omelia CR. Effect of Electrolyte Type on the Electrophoretic Mobility of Polystyrene Latex Colloids. Colloids Surf 1990;44:165–78.

Elimelech M, Gregory J, Jia X, Williams R. Particle deposition and aggregation: measurement, modeling, and simulation. Boston: Butterworth-Heinemann; 1995.

Guardia P, Batlle-Brugal B, Roca AG, Iglesias O, Morales MP, Serna CJ, et al. Surfactant effects in magnetite nanoparticles of controlled size. J Magn Magn Mater 2007;316: E756–9.

He YT, Wan JM, Tokunaga T. Kinetic stability of hematite nanoparticles: the effect of particle sizes. J Nanopart Res 2008;10:321–32.

Holthoff H, Egelhaaf SU, Borkovec M, Schurtenberger P, Sticher H. Coagulation rate measurements of colloidal particles by simultaneous static and dynamic light scattering. Langmuir 1996;12(23):5541–9.

Hristovski K, Baumgardner A, Westerhoff P. Selecting metal oxide nanomaterials for arsenic removal in fixed bed columns: from nanopowders to aggregated nanoparticle media. J Hazard Mater 2007;147:265–74.

Hu JH, Johnston KP, Williams RO. Nanoparticle engineering processes for enhancing the dissolution rates of poorly water soluble drugs. Drug Dev Ind Pharm 2004;30: 233–45.

Illés E, Tombácz E. The effect of humic acid adsorption on pH-dependent surface charging and aggregation of magnetite nanoparticles. J Colloid Interface Sci 2006;295:115–23.

Jekel MR. The stabilization of dispersed mineral particles by adsorption of humic substances. Water Res 1986;20:1543–54.

Kim EK, Walker HW. Effect of cationic polymer additives on the adsorption of humic acid onto iron oxide particles. Colloids Surf A Physicochem Eng Aspects 2001;194: 123–31.

Kretzschmar R, Holthoff H, Sticher H. Influence of pH and humic acid on coagulation kinetics of kaolinite: a dynamic light scattering study. J Colloid Interface Sci 1998;202:95-103.

Latham AH, Williams ME. Controlling transport and chemical functionality of magnetic nanoparticles. Acc Chem Res 2008;41:411–20.

Lurie M, Rebhun M. Effect of properties of polyelectrolytes on their interaction with particulates and soluble organics. Water Sci Technol 1997;36:93-101.

Majewski P, Thierry B. Functionalized magnetite nanoparticles — synthesis, properties, and bio-applications. Crit Rev Solid State and Mater Sci 2007;32:203–15.

Meyer G, Amer NM. Simultaneous measurement of lateral and normal forces with an optical-beam-deflection atomic force microscope. Appl Phys Lett 1990;57:2089–91.

Mylon SE, Chen KL, Elimelech M. Influence of natural organic matter and ionic composition on the kinetics and structure of hematite colloid aggregation: Implications to iron depletion in estuaries. Langmuir 2004;20(21):9000–6.

Oberdorster G, Oberdorster E, Oberdorster J. Nanotoxicology: an emerging discipline evolving from studies of ultrafine particles. Environ Health Perspect 2005;113: 823–39.

Ojamae L, Aulin C, Pedersen H, Kall PO. IR and quantum-chemical studies of carboxylic acid and glycine adsorption on rutile TiO2 nanoparticles. J Colloid Interface Sci 2006;296:71–8.

Pelley AJ, Tufenkji N. Effect of particle size and natural organic matter on the migration of nano- and microscale latex particles in saturated porous media. J Colloid Interface Sci 2008;321(1):74–83.

Phenrat T, Saleh N, Sirk K, Tilton RD, Lowry GV. Aggregation and sedimentation of aqueous nanoscale zerovalent iron dispersions. Environ Sci Technol 2007;41: 284–90.

Plaza RC, Quirantes A, Delgado AV. Stability of dispersions of colloidal hematite/yttrium oxide core-shell particles. J Colloid Interface Sci 2002;252(1):102–8.

Ramos-Tejada MM, Ontiveros A, Viota JL, Duran JDG. Interfacial and rheological properties of humic acid/hematite suspensions. J Colloid Interface Sci 2003;268(1): 85–95.

Regazzoni AE, Blesa MA, Maroto AJG. Interfacial properties of zirconium dioxide and magnetite in water. J Colloid Interface Sci 1983;91:560–70.

Sander S, Mosley LM, Hunter KA. Investigation of interparticle forces in natural waters: effects of adsorbed humic acids on iron oxide and alumina surface properties. Environ Sci Technol 2004;38:4791–6.

Schudel M, Behrens SH, Holthoff H, Kretzschmar R, Borkovec M. Absolute aggregation rate constants of hematite particles in aqueous suspensions: a comparison of two different surface morphologies. J Colloid Interface Sci 1997;196:241–53.

Si SF, Li CH, Wang X, Yu DP, Peng Q, Li YD. Magnetic monodisperse Fe_3O_4 nanoparticles. Cryst Growth Des 2005;5:391–3.

Sverjensky DA, Sahai N. Theoretical prediction of single-site enthalpies of surface protonation for oxides and silicates in water. Geochim Cosmochim Acta 1998;62: 3703–16.

Teja AS, Koh PY. Synthesis, properties, and applications of magnetic iron oxide nanoparticles. Prog Cryst Growth Charact Mater 2009;55:22–45.

Tipping E, Higgins DC. The effect of adsorbed humic substances on the colloid stability of hematite particles. Colloids Surf 1982;5:85–92.

Tombacz E, Filipcsei G, Szekeres M, Gingl Z. Particle aggregation in complex aquatic systems. Colloids Surf A Physicochem Eng Aspects 1999;151:233–44.

Tombacz E, Libor Z, Illes E, Majzik A, Klumpp E. The role of reactive surface sites and complexation by humic acids in the interaction of clay mineral and iron oxide particles. Org Geochem 2004;35:257–67.

Vanoss CJ. Interfacial forces in aqueous media. New York: Marcel Dekker; 1994.

Vanoss CJ, Chaudhury MK, Good RJ. Interfacial Lifshitz–Vanderwaals and polar interactions in macroscopic systems. Chem Rev 1988;88:927–41.

Vanoss CJ, Ju L, Chaudhury MK, Good RJ. Estimation of the polar parameters of the surface-tension of liquids by contact-angle measurements on gels. J Colloid Interface Sci 1989;128:313–9.

Vermeer AWP, van Riemsdijk WH, Koopal LK. Adsorption of humic acid to mineral particles. 1. Specific and electrostatic interactions. Langmuir 1998;14:2810–9.

Verwey EJW, Overbeek JTG. Theory of the stability of lyophobic colloids. Amsterdam: Elsevier; 1948.

Verrall KE, Warwick P, Fairhurst AJ. Application of the Schulze-Hardy rule to haematite and haematite/humate colloid stability. Colloids Surf A Physicochem Eng Aspects 1999;150(1–3):261–73.

Walker HW, Bob MM. Stability of particle flocs upon addition of natural organic matter under quiescent conditions. Water Res 2001;35:875–82.

Wan SR, Huang JS, Yan HS, Liu KL. Size-controlled preparation of magnetite nanoparticles in the presence of graft copolymers. J Mater Chem 2006;16: 298–303.
Wei X, Viadero JRC. Synthesis of magnetite nanoparticles with ferric iron recovered from acid mine drainage: implications for environmental engineering. Colloids Surf A Physicochem Eng Aspects 2007;294:280–6.
Zhang QA, Thompson MS, Carmichael-Baranauskas AY, Caba BL, Zalich MA, Lin YN, et al. Aqueous dispersions of magnetite nanoparticles complexed with copolyether dispersants: experiments and theory. Langmuir 2007;23:6927–36.
Zukoski CF, Saville DA. The Interpretation of Electrokinetic Measurements Using a Dynamic-Model of the Stern Layer .1. The Dynamic-Model. J Colloid Interface Sci 1986;114(1):32–44.